THE JOURNAL OF PHYSICAL CHEMISTRY B

Article

pubs.acs.org/JPCB

Cation and Anion Transport in a Dicationic Imidazolium-Based Plastic Crystal Ion Conductor

Bryce E. Kidd, Mark D. Lingwood,[†] Minjae Lee,[‡] Harry W. Gibson, and Louis A. Madsen*

Department of Chemistry and Macromolecules and Interfaces Institute, Virginia Tech, Blacksburg, Virginia 24061, United States

ABSTRACT: Here we investigate the organic ionic plastic crystal 1,2-bis[*N*-(*N*′-hexylimidazolium-d_2(4,5))]ethane $2PF_6^-$ in one of its solid plastic crystal phases by means of multinuclear solid-state (SS) NMR and pulsed-field-gradient NMR diffusometry. We quantify distinct cation and anion diffusion coefficients as well as the Arrhenius diffusion activation energies (E_a) in this *dicationic* imidazolium-based plastic crystal. Our studies suggest a change in transport mechanism for the cation upon varying thermal and magnetic treatment (9.4 T), evidenced by differences in cation and anion E_a. Moreover, variable temperature ^{2}H SSNMR line shapes support a change in local molecular environment upon slow cooling in B_0. We quantify the percentage of mobile anions as a function of temperature with ^{19}F SSNMR, wherein two distinct spectral features are present. We also comment on the Arrhenius pre-exponential factor for diffusion (D_0), giving insight into the number of degrees of freedom for transport for both cation and anion as a function of thermal treatment. Given the breadth and depth of our measurements, we propose that bulk ion transport is dominated by anion diffusion in ionic-liquid-like domain boundaries separating crystallites. This study elucidates fundamental properties of this plastic crystal, and allows for a more general and deeper understanding of ion transport within such materials.

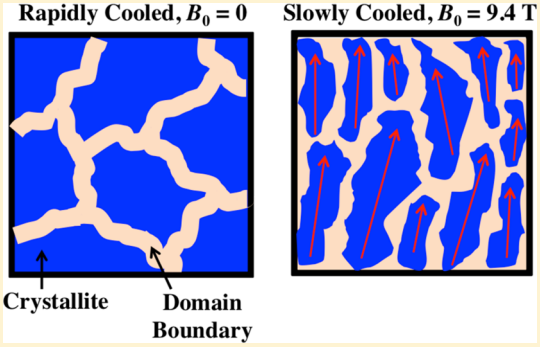

INTRODUCTION

Solid-state electrolytes, such as the perfluorosulfonate ionomer Nafion, have garnered much interest in the past decades for use in applications ranging from batteries to fuel cells.[1] Not only are new applications emerging, but new phenomena are being unveiled in these complex systems.[2] From a battery and fuel cell standpoint, a highly conductive stable matrix that allows fast charge transport from anode to cathode is required, and this conduction arises from intrinsic properties of the solid-state electrolyte. While ionic polymers such as Nafion are exceptional solid-state electrolytes, ion conduction is highly dependent on small volatile molecules (usually water) to mediate charge transport. This dependence on a volatile small molecule results in reduction of conductivity at elevated temperatures when the small molecule evaporates out of the electrolyte matrix.[3]

In contrast, a relatively new class of solid-state electrolytes known as organic ionic plastic crystals (OIPCs) have shown competitive ionic conductivity (10^{-3} S cm^{-1}) without some of the disadvantages of polymer electrolyte conductors. Similar to ionic liquids (ILs), OIPCs are electrolytes consisting purely of cations and anions. At room temperature (25 °C), an IL is a liquid salt, while an OIPC is a solid salt.[4] Unlike ILs, OIPCs exhibit efficient packing through long-range crystalline order of ions but have short-range disorder where isotropic states (i.e., isotropic rotational mobility of the cation and/or anion about one or more axes) exist below the melting temperature (T_m).[4,5] OIPCs have generated great interest due to their high ionic conductivity in one or more solid phases, which is attributed to joint rotational and translational motions within the crystalline lattice (i.e., rotator phase).[4,5] Many OIPCs possess multiple high enthalpy first-order solid−solid phase transitions below T_m, and conductivity tends to increase in the higher temperature phases.[4−7]

It is well-known that ion conduction within an ionic solid can occur through the classical "ion hopping" mechanism, whereby open vacancies within the crystalline lattice can promote diffusion.[8] If vacancies are present, charge neutrality must be conserved, so for every vacant cation, there must be a vacant anion within the lattice (commonly known as Schottky disorder).[8] In conjunction with conductivity and differential scanning calorimetry (DSC),[9] positron annihilation lifetime spectroscopy (PALS) studies[10] on OIPCs have shown relationships between the size and number of vacancies as a function of temperature, as well as discontinuous changes in the free volume of vacancies. Such behavior supports the ion hopping mechanism, as strong evidence suggests correlations between sizes of individual cations/anions, cation−anion pairs, and free-volume changes within the crystalline lattice.[10] While this holds true for OIPCs composed of small cations and/or anions, large steric or ionic potential barriers in the crystalline lattice can make ion transport difficult for more bulky cations and anions. For a system in which fast ion conduction is observed but cannot reasonably occur within the crystalline lattice, one must rethink the ion transport mechanism.

Because OIPCs are polycrystalline materials, grain boundaries on the nanometer-to-micrometer scale are naturally

Received: August 23, 2013
Revised: February 4, 2014
Published: February 4, 2014

   dx.doi.org/10.1021/jp4084629 | *J. Phys. Chem. B* 2014, 118, 2176−2185

Scheme 1. Synthesis of 1,2-Bis[*N*-(*N*′-hexylimidazolium-d_2(4,5))]ethane $2PF_6^-$ [6,7]

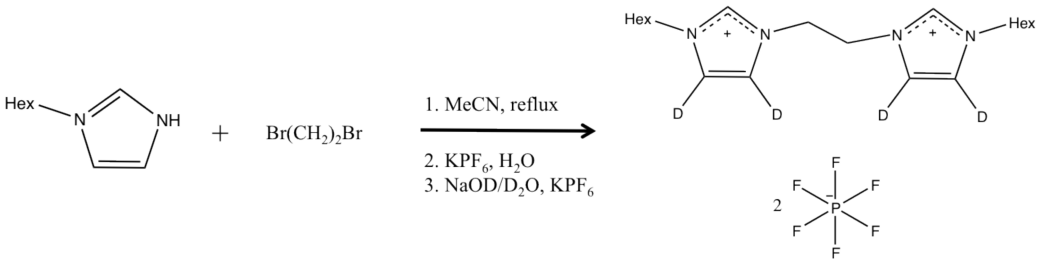

present. In general, grain boundaries form as a result of a mismatch in crystallite orientations in a polycrystalline material. Synthesis,[11] crystallite nucleation when cooling from above T_m,[12] thermal treatment,[11] and small applied forces[4] may induce and alter the size and number of grain boundaries present in a polycrystalline material. Previous work by Dosseh et al.[13] showed that molecular plastic crystals, such as 1,4-dioxane (T_m = 11 °C), cyclohexanol (T_m = 25 °C), cyclohexane (T_m = 7 °C), pivalic acid (T_m = 37 °C), and succinonitrile (T_m = 58 °C), melt at the grain boundary up to 10° below the bulk T_m. This is commonly known as the premelting phenomenon and occurs at the surface of a crystallite where gradual melting prior to T_m occurs. Through variable temperature ^{1}H SSNMR, Dosseh et al. observed a two-component system with a narrow signal centered on top of a broad signal. The narrow and broad signals were assigned to material in the grain boundary and crystallite, respectively. Approaching T_m caused the broad signal to diminish, accompanied by an increase in narrow signal.[13] For OIPCs, similar NMR spectral features have been reported for pure and doped forms of the materials. However, such spectral features are highly dependent on the cation−anion pair and concentration of dopant. While collections of dynamic crystalline defects (i.e., vacancies) can influence ion transport within OIPCs, grain boundaries (nm to μm in size) between abutting crystallites that contain noncrystalline ions can also contribute to ion transport. For OIPCs, collections of defects have been regarded as heterogeneous and dynamic (i.e., amorphous domain boundaries), wherein the bulk material is composed of an amorphous and crystalline component.[14] In the context of this work, we will refer to nm to μm length scale amorphous phase components, whether due to abutting of crystal grains or due to dynamic defects, as "domain boundaries".

Diffusion through the domain boundary represents an interesting way to think about ion transport within polycrystalline materials (and other materials). Since domain boundaries do not represent the lowest free energy state, usually only a small fraction of the total number of cations and anions reside within the domain boundary, and thus, the molecules in the domain boundary may give a low contribution to the overall material conductivity. The Nernst−Einstein equation[9]

$$\sigma = \frac{(D_+c_+ + D_-c_-)q^2}{kT} \quad (1)$$

where σ is the conductivity, $D_\pm$ are the diffusion coefficients for cation (+) and anion (−), $c_\pm$ are the concentrations of each charge carrier, q is the unit charge of the carrier, and kT is the average thermal energy (k is Boltzmann's constant and T is temperature), shows us that traditionally the contribution to the conductivity from domain boundaries should be small. It can be seen that σ linearly depends on each of the quantities $D_\pm$ and $c_\pm$. However, in order to optimize OIPCs, it is imperative to fully understand $D_\pm$ in both the crystalline component and domain boundaries of these materials. Domain boundary diffusion represents one diffusion pathway in OIPCs, and the local energetics associated with $D_\pm$ are not well understood. Variable temperature conductivity is commonly used to obtain translational activation energies (E_a); however, such measurements lack chemical specificity. In conjunction with chemically specific PFG-NMR diffusometry (discussed below), the Arrhenius equation

$$D = D_0 e^{-E_a/kT} \quad (2)$$

allows analysis of the T-dependent cation and anion diffusion coefficient D, thus giving insight into local energetics (i.e., activation energy E_a) on the prediffusion (~1 ps) time scale, commonly referred to as the inertial or ballistic time scale.[15,16] D_0 can be described as diffusion at infinite temperature or the "barrierless" diffusion coefficient, and kT is the average thermal energy. A deeper investigation on the prediffusion length scale allows understanding of collective interactions that govern the transport of small molecules in various environments, particularly environments where a crystalline lattice does not exist but diffusion occurs.

While DSC, conductivity, PALS, and X-ray diffraction have been used extensively to understand the OIPCs studied thus far, analyzing chemically specific transport properties, such as D, E_a, and D_0, will bring a more comprehensive understanding of ion transport and local energetics. Previously, we measured separate cation and anion diffusion coefficients for free ILs, such as [C_2mim][TfO], [C_2mim][BF_4], [C_4mim][TfO], and [C_4mim][BF_4], to better understand ion associations within the polymeric electrolyte membrane (PEM) Nafion 117 (N117) as a function of water content χ_{water} (n_{water}:n_{ILs}).[17] We showed anomalous cation diffusion ($D_{cation} > D_{anion}$ by 30−50%) at low χ_{water} values as a result of anion aggregations, and water-screened ionic interactions at high χ_{water} values. Thus, within pure ionic systems, such associations may influence E_a of cations, anions, and solvents. D_0 can also be used to report on the configurational degrees of freedom (i.e., entropic contributions) governing diffusion of various mobile species.[15,16,18,19]

Here we employ multinuclear pulsed-field-gradient (PFG) NMR diffusometry to report on the diffusion of cations and anions as well as their local energetics (i.e., E_a), and we use multinuclear static solid-state NMR to spectroscopically observe both crystalline and noncrystalline ions. We show that the ionic species that dominate bulk conductivity reside within the domain boundary. Strikingly, cooling in the strong spectrometer magnetic field (B_0) of 9.4 T induces a weak alignment of crystallites such that the E_a for the cation increases from 14 to 39 kJ mol^{-1}. Additionally, we quantify the

dx.doi.org/10.1021/jp4084629 | J. Phys. Chem. B 2014, 118, 2176−2185

percentage of mobile anions as a function of temperature from variable temperature ^{19}F SSNMR, where two distinct spectral features are observed. We also comment on the pre-exponential factor (D_0), giving insight into the configurational degrees of freedom[15,16,18,19] and how the local environment affects E_a for both cation and anion as a function of thermal treatment.

EXPERIMENTAL SECTION

Sample Preparation. The deuterated analog of bis[*N*-(*N*′-hexylimidazolium)] salt was synthesized in three steps (Scheme 1):

First, the quaternization coupling reaction of 1-hexylimidazole (2 mol equiv) with dibromoalkane (1 mol equiv) was carried out, followed by PF_6^- exchange in water, as previously reported.[6,7] Deuterium exchange on the 4- and 5-positions of the imidazolium was done with 10 wt % NaOD solution in D_2O. The final product was precipitated in aqueous (H_2O) saturated KPF_6 solution and was a white crystalline solid at room temperature (25 °C). It should be noted that the labile 2-position had also been deuterated but reverted back to protonated form upon introduction of the saturated aqueous KPF_6 solution.[6,7] Drying in a vacuum oven for 24 h with heat gave the colorless crystalline deuterated product with a quantitative yield. The material (~30 mg) was loaded into a 5 mm outer diameter glass bulb, heated in an oil bath under a vacuum to 210 °C (T_m = 196 °C), and degassed under a vacuum to prevent degradation. Upon cooling to room temperature (25 °C) and leaving under a vacuum overnight, the glass bulb was sealed with an oxygen/natural gas torch.

Variable Temperature Solid-State NMR. All ^{1}H/^{2}H/^{19}F variable temperature (^{1}H, 207−25 °C; ^{2}H, 196− 30 °C; ^{19}F, 205−40 °C) SSNMR experiments were performed using a 400 MHz Bruker Avance III WB NMR spectrometer, equipped with a two-channel HX wide-line static solids probe (Bruker HP WB 73A). The sample was allowed to equilibrate at each temperature for 30 min prior to spectral acquisition. The quadrupolar (solid) echo pulse sequence[20] was used to acquire ^{2}H NMR spectra, and a simple pulse-acquire sequence was used to acquire ^{1}H/^{19}F NMR spectra. For this study, a series of deuterated standards, hexamethylbenzene-d_{18} (HMB-d_{18}) (T_m = ~167 °C) purchased from Sigma Aldrich with >99% purity, urea-d_4 (T_m = ~133 °C) purchased from Sigma Aldrich with >98% purity, and the liquid crystal 2,5-bis-(*p*-hydroxyphenyl)-1,3,4-oxadiazole (ODBP-Ph-C$_7$-d_6) [phase map: crystal to smectic Y (148 °C), smectic Y to B2 (166 °C), B2 to biaxial nematic (173 °C), biaxial nematic to uniaxial nematic (215 °C), and uniaxial nematic to isotropic (222 °C)][21,22] were used to calibrate the probe at multiple temperatures, as each of these materials displays distinct changes in quadrupole splitting $\Delta\nu_Q$ at their respective phase transitions.

Variable Temperature Pulsed-Field-Gradient NMR. All variable temperature (75−65 °C, PFG probe temperature maximum is 80 °C) ^{1}H (cation diffusion) and ^{19}F (anion diffusion) PFG-NMR diffusometry experiments were performed using a 400 MHz Bruker Avance III WB NMR spectrometer, equipped with an MIC probe coupled to a Diff60 single-axis (*z*-axis) gradient system. In the PFG-NMR diffusometry experiment, the Stejskal−Tanner equation (eq 3)[23] was fit to the measured signal amplitude I as a function of gradient strength g

$$I = I_0 e^{-D\gamma^2 g^2 \delta^2 (\Delta - (\delta/3))} \quad (3)$$

where I_0 is the signal amplitude at g = 0, γ is the gyromagnetic ratio, δ is the effective gradient pulse length, Δ is the diffusion time between gradient pulses, and D is the self-diffusion coefficient.[23] The simple and robust pulsed-gradient stimulated echo (PGSTE) sequence was used with $\pi/2$ pulse lengths of 7 and 7.1 μs for cation (^{1}H) and anion (^{19}F), respectively. A repetition time of 1.3 s, a diffusion time of Δ = 35 ms, and acquisition times of 15 ms (cation) and 10 ms (anion) were used for cation and anion diffusion measurements. A sinusoidal gradient pulse length of δ = 3.14 ms (actual pulse length = 1.57 × 2.00 ms, where 2.00 ms is the effective pulse length as if the pulse were rectangular) and maximum gradient strength of 1850 G cm^{-1} were used to achieve 80% signal attenuation in eight steps. Sufficient signal-to-noise ratio (SNR) for each data point was achieved with 64 and 320 scans for cation and anion, respectively. The PGSTE parameters were calibrated as previously reported.[24] Cation and anion spin−lattice relaxation times (T_1) in phase S_3 were measured using the inversion−recovery pulse sequence to be 140 and 630 ms, respectively. Cation and anion spin−spin relaxation times (T_2) were measured using the Carr−Purcell−Meiboom−Gill pulse sequence to be 6 and 48 ms, respectively.

RESULTS AND DISCUSSION

The DSC trace for the present OIPC (Figure 1) displays three distinct solid−solid phase transitions, where each phase has

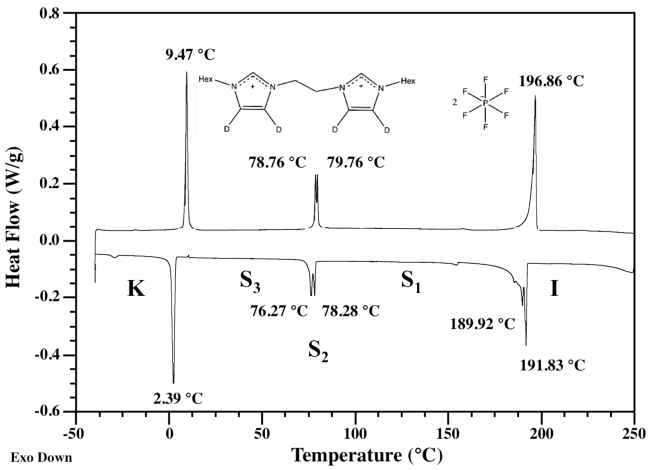

Figure 1. Differential scanning calorimetry (DSC) trace (heating and cooling rate 5 K min^{-1}, N_2) of the ionic compound 1,2-bis[*N*-(*N*′-hexylimidazolium-d_2(4,5))]ethane $2PF_6^-$ used in this study. K (crystal), S_3, S_2, and S_1 all represent solid phases, and I represents the isotropic melt.

distinct ion transport behavior.[6,7] High T_m's for this class of OIPCs are due to the many hydrogen−fluorine contacts, reported from single crystal X-ray diffraction.[7] For the present study, we studied phases S_3 through I using variable temperature multinuclear NMR experiments and studied phase S_3 only using variable temperature multinuclear PFG-NMR diffusometry experiments, due to NMR probe temperature limitations (80 °C).

Temperature-Dependent ^{2}H NMR Studies. Figure 2 shows a representative ^{2}H NMR spectrum obtained at room temperature (25 °C, phase S_3) before heating the sample in the magnetic field, which displays an isotropic distribution of crystallite orientations with B_0, thus forming the well-known Pake powder pattern.[25] Such a spectrum can be described by

dx.doi.org/10.1021/jp4084629 | J. Phys. Chem. B 2014, 118, 2176−2185

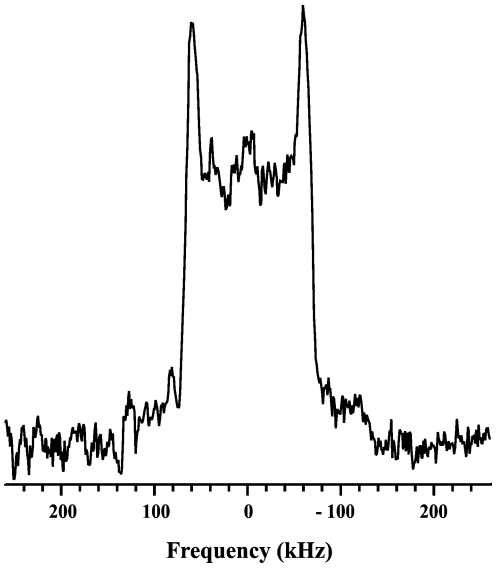

Figure 2. Room temperature (25 °C) ^{2}H NMR measurement of OIPC powder (before heating in the magnetic field) that displays the well-known Pake pattern, confirming a random orientation of crystallites with respect to B_0. We observe ν_Q = 121 kHz, which translates to C_Q = 161 kHz.

$$\Delta\nu_Q(\theta_Q) = 3\pi C_Q \times \frac{1}{2}(3\cos^2\theta_Q - 1) \quad (4)$$

where θ is the angle of the C−^{2}H bond (^{2}H being a spin I = 1 quadrupolar nucleus) with respect to the spectrometer field B_0, C_Q is the quadrupole coupling constant, and $\Delta\nu_Q$ is the quadrupolar (spectral) splitting for a given nucleus oriented at angle θ.[26] C_Q represents the magnitude of the nuclear quadrupole moment interaction with the electric field gradient, which is sensitive to the local environment. We observe a splitting ν_Q between the two singularities (θ_Q = 90°) of 121 kHz. Since ^{2}H is spin I = 1, $\nu_Q = 3C_Q/4$,[27] thus C_Q = 161 kHz. Figure 2 also shows a small single peak centered at 0 Hz, which likely arises from a small (∼1%) population of motionally averaged mobile cations.

We use temperature-dependent ^{2}H NMR to probe the imidazolium dynamics through all solid phases and into the isotropic phase. Figure 3 shows ^{2}H NMR spectra as a function of temperature (steps of 5−20 °C with 30 min equilibration for each step over the course of 16 h), in phases I, S_1, and S_3. When the OIPC is heated above T_m (196 °C), we observe a single narrow signal, indicating that the quadrupolar interactions average to zero due to rapid tumbling of molecules in the isotropic (melt) state. Upon cooling to 85 °C (phase S_1) in the magnetic field, we still observe a significant fraction of the isotropic phase, suggesting that isotropic tumbling of many cations occurs, even in the solid state. Two distinct spectral features, a narrow signal residing on a broad signal, occur at 50 °C (phase S_3). However, at 30 °C (phase S_3), the isotropic signal diminishes dramatically along with the broad flat shoulders, leaving behind a broad doublet ($\Delta\nu_Q \approx$ 120 kHz) due to an anisotropic distribution of crystallites. According to eq 4, and if there is an average alignment axis present for the crystallites, $\Delta\nu_Q$ should reduce by half when the alignment axis relative to the B_0 field is rotated to θ = 90°. Therefore, we tested this by manually rotating the sample 90° while still in the S_3 solid phase. The bottom trace of Figure 3 shows that $\Delta\nu_Q$ is approximately halved ($\Delta\nu_Q \approx$ 60 kHz) when θ = 90°. The

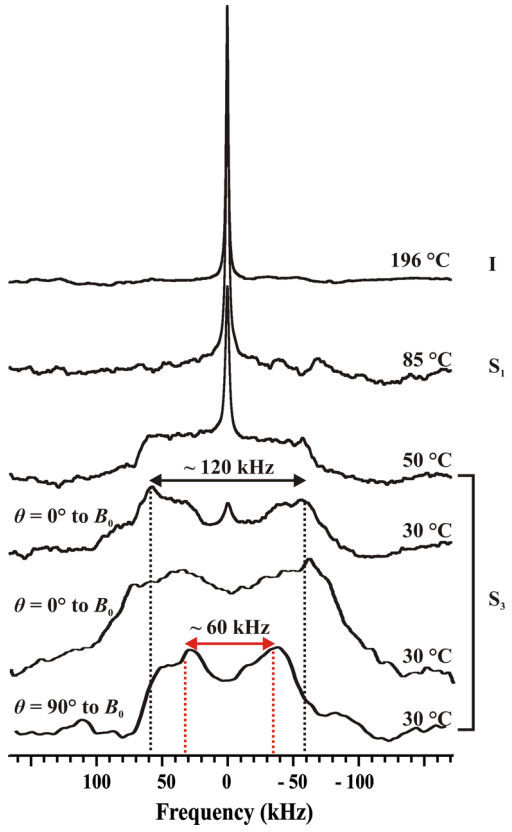

Figure 3. ^{2}H NMR spectra vs temperature displaying imidazolium orientation and dynamics in phases I, S_1, and S_3. One observes weak alignment upon cooling in the magnetic field, evidenced by the broad quadrupolar doublet in phase S_3 at 30 °C when θ = 0° followed by a reduction in $\Delta\nu_Q$ by approximately half when the sample is manually rotated to θ = 90°. The spectrum third from bottom at 30 °C was after initial cooling, while the lowest two spectra were for the subsequently melted sample that was then reoriented in the solid phase.

lowest two spectra in Figure 3 are after slow cooling and multiple thermal cycles, and the central signal is reduced relative to the broad signals and relative to the spectrum third from bottom, which was after initial cooling in the field. These results indicate that melting and then cooling in the magnetic field induces alignment of crystalline domains inside this material.

We propose a broadly distributed but anisotropic crystallite alignment upon melting and subsequent cooling in the presence of B_0. Alignment of the long axis of a molecule (i.e., the molecule has an aspect ratio >1) along the direction of a strong magnetic field B_0 has been observed for many liquid-crystalline (LC) systems[28] but not so far for an OIPC. Within a magnetically aligned LC phase, the molecules collectively align to minimize magnetic free energy. We propose a related effect for OIPCs composed of anisotropic crystallites. While OIPCs and LCs are quite different, molecular susceptibility anisotropy effects may extend to OIPC *crystallites* composed of aromatic rings (i.e., imidazolium). Crystallites can have an aspect ratio associated with them, and thus, magnetic susceptibility anisotropy may exist. We believe that crystallite alignment with B_0 begins immediately upon solidification from T_m but is not observed until lower temperatures due to imidazolium motional averaging. Figure 4 gives a conceptual illustration to depict realignment of the crystallites upon cooling in B_0. These ^{2}H NMR results are the first to show crystallite alignment

dx.doi.org/10.1021/jp4084629 | J. Phys. Chem. B 2014, 118, 2176−2185

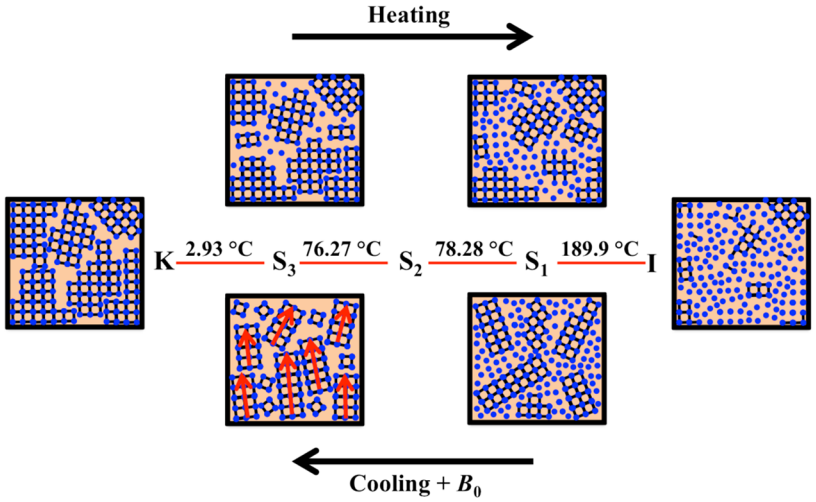

Figure 4. Illustration of crystallite realignment model in a magnetic field upon heating to phase I and cooling to phase S_3 (transition temperatures taken from DSC exotherm). Cooling in B_0 induces the formation of anisotropic crystallites such that the crystallite long axes (red arrows for emphasis) become biased along B_0.

within an OIPC induced by a strong magnetic field, carrying implications for orientational control of plastic crystal ion conductors. As with other systems,[2] enhanced transport can result from control of morphological alignment of elongated crystallite structures.

Temperature-Dependent ^{19}F and ^{1}H NMR. To augment our variable temperature ^{2}H NMR results, we investigate how anion (^{19}F) and cation (^{1}H) dynamics change as a function of temperature in the solid phases, as this gives molecular insights into bulk material properties. Figure 5 shows representative ^{19}F NMR spectra as a function of temperature (205−40 °C) in 20° increments. In the isotropic phase, we clearly observe the J_{PF} scalar coupling (i.e., doublet in Figure 5) between phosphorus and fluorine. This coupling constant, J_{PF} = 720 Hz, is exactly that observed in a standard solution of KPF_6. We note that the small doublet at −10 kHz with a splitting of 1 kHz cannot be from PF_6^- and could be a small sample impurity. However, we do not see this doublet in our T_2-weighted PFG spectrum (discussed below); thus, it could arise from some ^{19}F-containing material within our solids probe. Cooling the sample to phase S_1 drastically decreases the intensity of the isotropic signal, and a broad signal also emerges. We might be tempted to rationalize that the isotropic averaging occurs through the rotation of PF_6^- about the fixed crystalline lattice point (a rotator phase effect). However, such spectral features are observed for other OIPCs[11,29,30] and molecular crystals,[13] whose isotropic signal is suggested to be ions diffusing between crystallites (i.e., in domain boundaries), while the broad signal is suggested to be ions in a rigid environment (i.e., in crystallites). The ratio of narrow to broad signals changes continuously and strongly over this temperature range, also suggesting that the isotropic signal is not simply PF_6^- in fixed lattice positions. Thus, we assign the isotropic signal to PF_6^- within the domain boundary and the broad signal to crystalline PF_6^-.

We quantify the relative proportions of PF_6^- in the domain boundary and crystallite from Figure 5 through integration of the broad and narrow spectral components (Figure 6). To compensate for the area integrated below the isotropic signal (i.e., part of the broad signal), a reference area under the broad signal is subtracted from the isotropic region integral. At 190 °C (just below phase I), 40% of the PF_6^- anions (and by charge balance, the counter-cations) reside in the domain boundaries (narrow isotropic signal) while the remaining 60% reside in the crystallites (broad signal). With decreasing temperature, an exponential-like decrease in isotropic PF_6^- is observed. Although ionic conductivity measurements for the OIPC used in this study have not been reported, variable temperature σ values in the range 10^{-5}−10^{-14} S cm^{-1} were reported for the related materials 1,2-bis[*N*-(*N*′-nonylimidazolium)]ethane $2PF_6^-$, 1,2-bis[*N*-(*N*′-decylimidazolium)]ethane $2PF_6^-$, and 1,2-bis[*N*-(*N*′-dodecylimidazolium)]ethane $2PF_6^-$.[6] As discussed above, the Nernst−Einstein equation (eq 1) relates conductivity to the diffusion coefficients and concentrations of charge carrying species. Thus, the initially small percentage of fast tumbling PF_6^- and relatively small diffusion coefficient (discussed below) observed in the large temperature window (40−140 °C) can explain the initially low but accelerating increase in conductivity with T, as reported for other OIPCs.[6] Previous work by Dosseh et al. reported the premelting of polycrystalline materials at the surface of domain boundaries prior to T_m.[13] On the basis of the present variable temperature ^{19}F NMR results, we are apparently observing gradual melting of the material at the surface of the domain boundary until ∼150 °C when a more dramatic increase in "local melting" occurs as T approaches T_m.

Figure 7 shows variable temperature ^{1}H NMR. Two-component spectral features do not appear as cleanly as in our ^{19}F NMR results due to the spectral crowding and somewhat broad lines, but we observe clear spectral changes in phases S_1 and S_3. Dipolar couplings between protons contain the same orientation dependence with B_0, but we do not observe clean orientation dependence with respect to B_0 as in ^{2}H NMR, further emphasizing the advantage of isotopic labeling. Clearly, isotropic mobility exists well below T_m, consistent with our variable temperature ^{2}H NMR spectra, wherein an isotropic signal is observed even down to 25 °C. Note that a residual signal from protons 2 and 3 remains after the ^{2}H exchange reaction. The proton 2 and 3 signals differ by only 0.13 ppm at 400 MHz when measured in solution (acetone-d_6),[7] and thus, our lines are too broad to resolve them.

dx.doi.org/10.1021/jp4084629 | J. Phys. Chem. B 2014, 118, 2176−2185

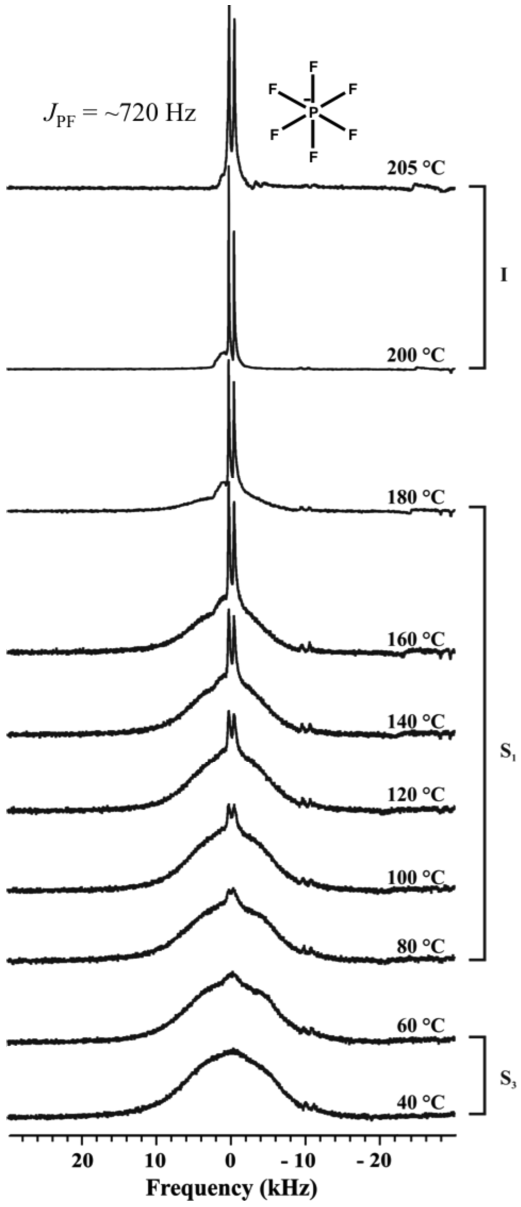

Figure 5. ^{19}F spectra as a function of temperature. Spectra at 205, 200, and 180 °C are decreased on the vertical scale by factors of 10, 10, and 4, respectively, relative to the other spectra. We observe an isotropic signal from phase I to phase S_3 with J_{PF} = 720 Hz, consistent with the PF_6^-. The isotropic signal indicates rapidly rotating and diffusing PF_6^- in the domain boundary, supporting ^{19}F PFG-NMR diffusometry. The broad signal corresponds to PF_6^- in crystallites.

Thermal and Magnetic Treatment. Previous work by Rana et al.[11] on the OIPC choline dihydrogen phosphate [choline][DHP] doped with phosphoric acid [H_3PO_4], trifluoromethanesulfonic acid [TfOH], and bis-trifluoromethanesulfonyl imide [HN(Tf)$_2$] showed that the thermal history of an OIPC critically affects macroscopic and microscopic properties. Changes were reported in ^{1}H NMR spectra for the pure material "as-prepared" and annealed (both with no dopants).[11] The ^{1}H NMR spectra at 100 °C for both materials displayed two distinct spectral components: a broad component (~35 kHz) representative of crystalline material and a narrow component (~300 Hz) representative of noncrystalline material. The narrow component was suggested to be diffusing cations. Annealing the material afforded the formation of less defective crystallites (i.e., less Schottky disorder) and/or fewer/smaller domain boundaries, as evidenced by the increase in the broad component (i.e., more crystalline material) and decrease in conductivity.[11]

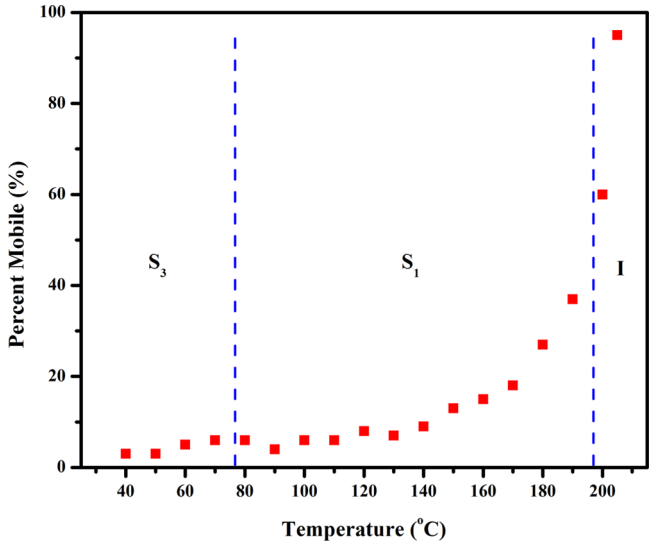

Figure 6. Percentage of mobile PF_6^- (i.e., in the domain boundary) as a function of temperature. We observe a gradual increase in percentage below the middle of phase S_1 and an exponential-like growth above 140 °C. The dotted lines represent the transition temperatures from DSC.

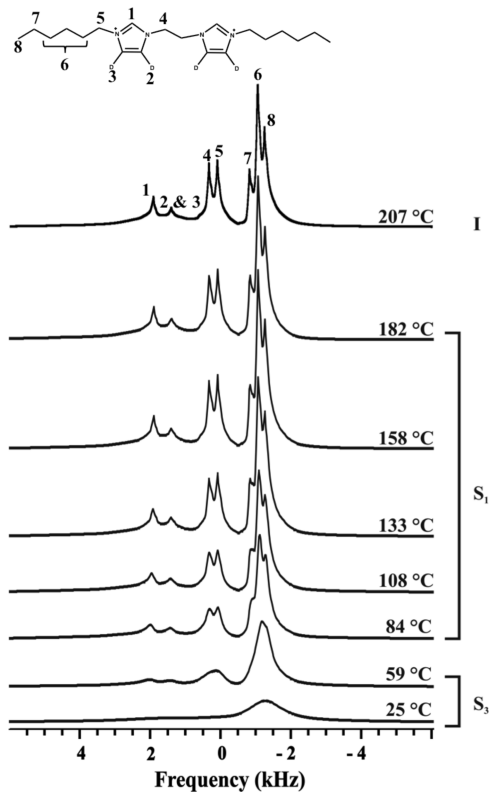

Figure 7. ^{1}H NMR spectra as a function of temperature. Above T_m, we clearly see all ^{1}H signals. An unresolved residual signal from protons 2 and 3 remains after the ^{2}H exchange reaction. We observe a change in spectral features when cooling in phase S_3, which is consistent with variable temperature ^{2}H NMR spectral changes in phase S_3.

dx.doi.org/10.1021/jp4084629 | J. Phys. Chem. B 2014, 118, 2176−2185

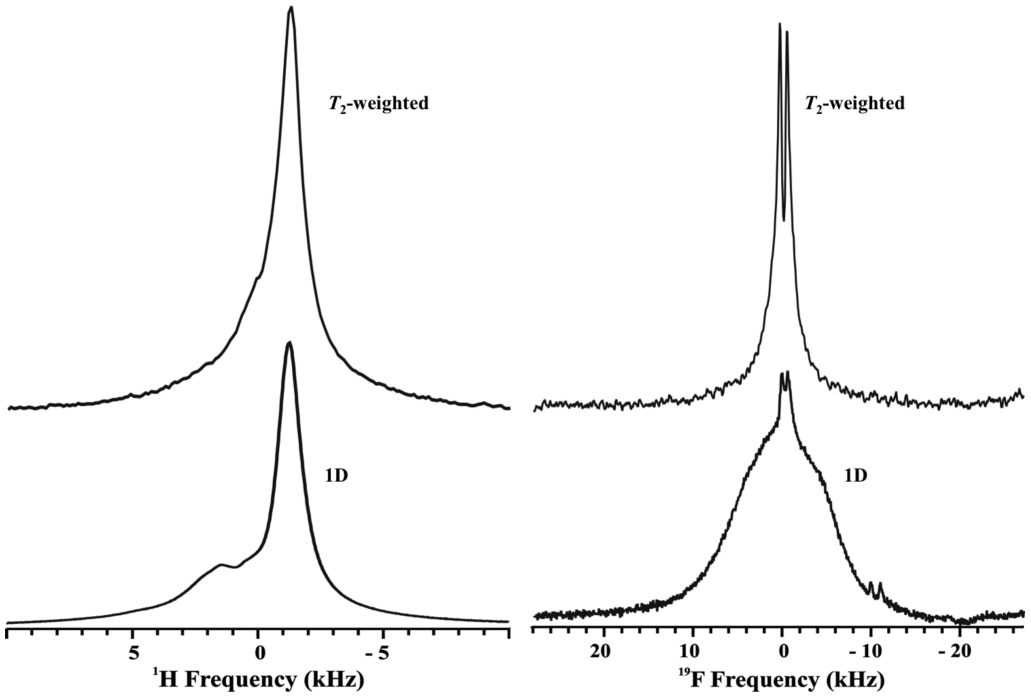

Figure 8. Comparison of static 1D and T_2-weighted PFG ^{1}H and ^{19}F spectra, all within phase S_3, emphasizing that PFG-NMR diffusometry measures only mobile cations and anions within this material. The T_2-weighted signals result from T_2 relaxation during the gradient pulse encoding periods. ^{1}H and ^{19}F T_2-weighted spectra were scaled vertically by factors of 137 and 52, respectively, relative to 1D spectra, to allow for easy comparison.

To study the effect of varying magnetic and thermal history on transport, we present a systematic study of ^{1}H and ^{19}F PFG-NMR diffusometry experiments with two different thermal treatments (slowly and rapidly cooled out of B_0) in conjunction with the magnetic treatment (slowly cooled in B_0) resulting in different observations in phase S_3. The magnetic treatment involved starting in the melt state in B_0 and then the temperature was decreased in steps of 5−20 °C with 30 min equilibration between steps, all while acquiring NMR data as in the ^{1}H, ^{2}H, and ^{19}F studies described above. Due to PFG-probe temperature limitations (maximum 80 °C), the B_0 aligned sample was transferred from the wide-line static solids probe to the PFG probe for diffusion measurements. The second treatment was to melt the material in an oil bath, remove it, and cool it quickly in air to room temperature (sample cool to touch within 10 min), thus erasing the crystallite alignment history outside of B_0. The third thermal treatment was to melt the material in an oil bath and allow it to cool to room temperature while held in the oil bath (≈2 h), resulting in a slow cooling thermal treatment outside of B_0.

Diffusion Coefficient vs Temperature. We conducted cation (^{1}H) and anion (^{19}F) PFG-NMR diffusometry experiments on the OIPC 1,2-bis[*N*-(*N*′-hexylimidazolium-d_2(4,5))]C_2H_4 $2PF_6^-$. The accessible PFG-NMR pulse sequence parameters δ and Δ depend on the OIPC relaxation time constants T_2 and T_1, respectively. In the PFG experiment, a T_2-weighted spectrum is produced (Figure 8) as a result of T_2 relaxation during the gradient pulse encoding periods. Thus, we do not observe signals with relatively short T_2 as we do with simple pulse-acquire spectra. The spectral components with short T_2 correspond to the slowly rotating material components, in this case the ions in the crystallites.

Figure 9 shows Arrhenius plots of temperature-dependent diffusion measurements between 75 and 67 °C (phase S_3) in 2° increments to allow measurement of E_a for the cation and anion. Note that the high precision (error in $D \leq \pm 6\%$) of these measurements allows for E_a determination over a relatively small T range. We extended this temperature window to 41 °C for one sample to verify that our measurements exhibit Arrhenius behavior over a wider temperature range.

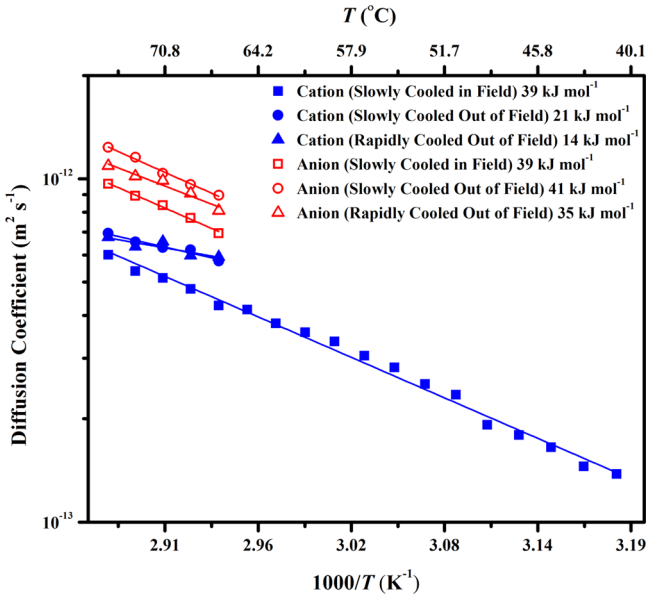

Figure 9. Temperature dependence of diffusion coefficient for both cation and anion as a function of thermal treatment and summary of all E_a values extracted from Arrhenius plots. Anion E_a changes fall within error as a function of thermal treatment, suggesting that the anion transport mechanism does not change significantly with respect to thermal treatment. Slow cooling in B_0 causes E_a for the cation to increase drastically to 39 kJ mol^{-1}, suggestive of a change in transport mechanism (local molecular environment). D and E_a errors are $\leq \pm 6\%$ and ± 5 kJ mol^{-1} using the statistics of the linear fit.

dx.doi.org/10.1021/jp4084629 | J. Phys. Chem. B 2014, 118, 2176−2185

Figure 9 is a compilation of all Arrhenius plots with respective E_a values for both cation and anion as a function of thermal treatment. Thermal treatment of the material is critical for the following measurements, as E_a is sensitive to thermally driven changes in D.

For OIPCs, we observe that magnetically driven changes in D can strongly supplement, or even outweigh, changes due to thermal cooling rate when starting from the melt state. Interestingly, both the cation and anion have E_a values of 39 kJ mol^{-1} in phase S_3 when the material is slowly cooled in B_0. However, when the material is slowly cooled outside of B_0, cation E_a decreases by a factor of 2 (39 to 21 kJ mol^{-1}), while anion E_a does not change, within error bars. This suggests that, after cooling out of B_0, the cation local (~1 nm) environment is influenced such that less energy is required for ion transport, while the anion's environment remains unchanged. When the sample is rapidly cooled outside of B_0, the anion E_a is unchanged, while the cation E_a appears to be lower than when slowly cooled outside of B_0, although these measurements are still within error. Rapid cooling should promote the formation of smaller or more defective crystallites (on the nm length scale) with more and/or larger domain boundaries (on the μm length scale), and this appears to manifest as a slight decrease in the activation energy for cation transport. The cation E_a change is larger when varying the magnetic cooling conditions (slow cooling in vs out of B_0) than when varying the cooling rate (rapid vs slow cooling out of B_0). These results indicate that the presence of a large magnetic field B_0, rather than cooling rate, dominates local energetic environment changes. This agrees with our ^{2}H observations and supports a crystallite orientation effect that strongly influences transport processes.

To further rationalize changes in local energetics experienced by the cation and anion within the domain boundary, we revisit the Arrhenius equation (eq 2). The pre-exponential factor, D_0, contains information about the local structure (i.e., the configurational degrees of freedom or the entropy of translation) of the system governing D for diffusing species.[15,16,18,19] For the polymer electrolyte Nafion, experimental[15] and molecular dynamics[16] investigations have shown that D_0 depends on water content (i.e., $\lambda = \mathrm{mol}_{H_2O}/\mathrm{mol}_{SO_3^-}$) within the nanophase-separated ion conducting channel.

We are currently working to extend the interpretation of D_0 and its quantitative significance to other materials. At the moment, we can gain at least a qualitative understanding of the relationship between E_a and D for the cation and anion by comparing their respective D_0 values. Figure 10 shows D_0 for the cation and anion as a function of thermal treatment. We note that our first investigation of D_0 in Nafion involved an inverted (reciprocal) error,[15] and we have corrected that in these analyses.

It can be seen that the D_0 changes for the anion with respect to thermal treatment fall within measurement error, suggesting that the degrees of freedom do not change, i.e., the available anion local configurations do not change significantly with thermal treatment. Surprisingly, the cation D_0 is largest when the material is slowly cooled in B_0 (i.e., higher translational entropy, less ordered environment). Cation and anion E_a values as a function of thermal treatment might suggest D_0 to be the largest when the material is rapidly cooled out of B_0 (i.e., least restricted cation environment) and smallest when the material is slowly cooled in B_0 (i.e., most restricted cation environment).

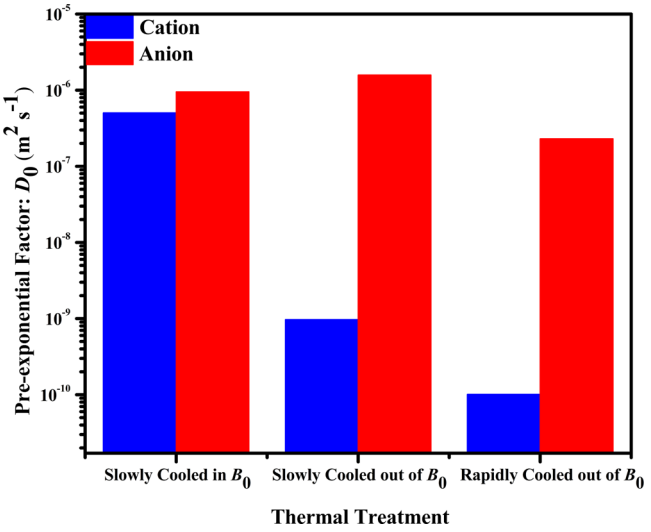

Figure 10. Cation and anion D_0 as a function of thermal treatment. Anion D_0 changes fall within the measurement error, suggesting that the local configurational degrees of freedom do not change with thermal treatment. The cation D_0 decreases by 3−4 orders of magnitude from slowly cooled in B_0 to cooled out of B_0. The D_0 error is estimated to be ±50%.

However, cation and anion D_0 values do not reflect such a rationale.

When contemplating the larger cation D_0 upon slowly cooling in B_0, we can consider the alignment of crystallites (Figure 4) observed when the material is slowly cooled in B_0. In liquid crystals, one observes a gain in translational entropy, compared to the isotropic phase, upon alignment of anisotropic species.[31] If the anisotropic cation is aligned in anisotropic cavities formed between the crystallites (anisotropic domain boundaries), then its translational entropy may increase relative to randomly shaped (isotropic) domain boundaries. Thus, slowly cooling in B_0 may increase cation translational entropy (i.e., D_0) and decrease E_a. Aligning in B_0, however, would not influence the anion local domain boundary dynamics or translational entropy, since PF_6^- is octahedral (i.e., nearly spherical). We are continuing to explore the significance of D_0 in this and other systems, and hope to provide further quantitative insight in the future.

Domain Boundary Restricted Diffusion. As stated above, an amorphous domain boundary can exist within these materials. We may further understand how the amorphous domain boundary influences ion transport by experimentally probing ~μm length scale environments using an NMR restricted diffusion study.[32−34] This method has shown previous utility in probing restrictive environments in solid-state electrolytes, where μm length scale morphological effects can influence small molecule/ion transport properties.[34] In the PFG-NMR diffusometry experiment, D vs diffusion time Δ will show a flat dependence (slope = 0) if the root-mean-square displacement $\langle r^2 \rangle$ is substantially smaller or larger than the size of the domain containing the diffusing species. If the diffusing species samples morphological restrictions, such as crystallite walls, during Δ, a decrease in D with increasing diffusion time Δ can appear, also known as restricted diffusion. Figure 11 representatively shows anion D vs Δ at 75 °C (slowly cooled in B_0) in a Δ range of 10−200 ms, thus enabling us to probe diffusion lengths from 0.1 to 0.4 μm.

dx.doi.org/10.1021/jp4084629 | J. Phys. Chem. B 2014, 118, 2176−2185

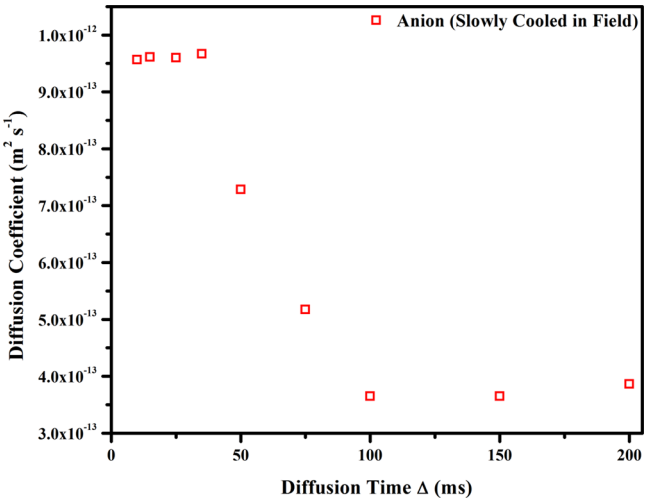

Figure 11. Anion D as a function of diffusion time Δ probes 0.1−0.4 μm length scales. A sharp decrease in D as a function of Δ indicates restricted diffusion when $\Delta \geq 50$ ms, giving an average domain boundary dimension of ∼0.2 μm.

We observe a sharp decrease in D as a function of Δ to a plateau that is a factor of 3 smaller in D, indicating strong restricted diffusion. On the basis of the root-mean-square displacement, also known as the diffusion length $\langle r^2 \rangle^{1/2} = (2D\Delta)^{1/2}$, an average domain boundary dimension of ∼0.2 μm is present within this OIPC. This calculated rough dimension assumes a model of spherical cavities with limited pathways between them.[32,33] Since we do not know the exact symmetry of the domains or crystallites, this will require further study (e.g., anisotropic restricted diffusion) to determine the crystallite and domain boundary geometries and dimensions. However, since we are probing D vs Δ along the proposed alignment axis of the crystallites, it is likely that 0.2 μm represents the length of the crystallites along that axis.

Since cation and anion local interactions govern the measured diffusion coefficients, we can take the perspective that essentially an ionic liquid exists in the domain boundary, and thus use our experimentally determined D values to evaluate intrinsic properties of the ionic microphase within the domain boundary, such as viscosity η and cation/anion hydrodynamic radii r_H, using the well-known Stokes−Einstein equation[35,36]

$$D = \frac{kT}{6\pi\eta r_H} \quad (5)$$

wherein kT is the average thermal energy (k is Boltzmann's constant and T is temperature), η is the viscosity of the medium, and r_H is the hydrodynamic radius of the diffusing species. As previously reported, PF_6^- should have r_H = 0.25 nm.[37] Knowing this value allows us to calculate a local viscosity η = 4.2 Pa·s and cation r_H = 0.41 nm. This viscosity is similar to those for viscous ionic liquids with relatively large ions, as is the cation in this study.[38] On the basis of the Stokes−Einstein relation, the measured cation and anion diffusion coefficients in the present material result from essentially a viscous IL residing in the domain boundary.

CONCLUSIONS

We have investigated the OIPC 1,2-bis[N-(N'-hexylimidazolium-d_2(4,5))]C_2H_4 $2PF_6^-$ by means of multinuclear variable temperature SSNMR and PFG-NMR diffusometry. This study uncovers new aspects of ion associations and transport in this OIPC and presents a rich combination of NMR techniques that promises to give further insights into such conducting materials. We show the importance of deuterium labeling these materials by using the C−^{2}H quadrupole coupling to spectrally observe an induced crystallite alignment upon slowly cooling in a 9.4 T magnetic field. This phenomenon has not been previously reported for any OIPC. Moreover, a change in local transport mechanism (molecular energetics) for the cation occurs in phase S_3 depending on thermal and magnetic treatment, evidenced by a change in E_a (14−39 kJ mol^{-1}), from the rapidly cooled case to when we slowly cool the sample in B_0. Changes in E_a as a function of thermal treatment for the anion fall within measurement error, suggesting that the transport mechanism of the anion does not significantly change. From variable temperature ^{19}F SSNMR, we also propose that the ion conduction for this OIPC is dominated by anion transport via domain boundaries, and we quantify the fraction of anions in domain boundaries versus those in crystallites. Utilization of the Stokes−Einstein equation yields a cation r_H = 0.41 nm and viscosity η = 4.2 Pa·s, suggestive of a viscous IL moving through domain boundaries. Structurally similar ILs have viscosities within this range.[38] Finally, a restricted diffusion study reveals an ∼0.2 μm dimension of restriction for ions in these domain boundaries.

Further studies on these materials are ongoing, including E_a measurements for the cation and anion within all phases, and the study of materials with different structures. While these OIPCs do not exhibit remarkable conductivities, doping with small amounts of lithium or sodium salts could potentially enhance conductivity and bring about new electrolyte applications, as previously observed for other OIPCs.[4,5,39−43]

AUTHOR INFORMATION

Corresponding Author

*E-mail: lmadsen@vt.edu.

Present Addresses

†(M.D.L.) Department of Chemistry, Saint Mary's College of California, Moraga, CA 94556.

‡(M.L.) Department of Chemistry, Kunsan University, 1170 Daehangno, Gunsan, South Korea 573-701.

Notes

The authors declare no competing financial interest.

ACKNOWLEDGMENTS

This work was supported by the National Science Foundation under award number CHE 1057797. Any opinions, findings, and conclusions or recommendations expressed in this material are those of the author(s) and do not necessarily reflect the views of the National Science Foundation (NSF). This material is also based upon work supported in part by the U.S. Army Research Office under Grant W911NF-07-1-0452 Ionic Liquids in Electro-Active Devices (ILEAD) MURI.

REFERENCES

(1) Mauritz, K. A.; Moore, R. B. State of Understanding of Nafion. *Chem. Rev.* **2004**, *104*, 4535−4585.

(2) Li, J.; Park, J. K.; Moore, R. B.; Madsen, L. A. Linear Coupling of Alignment with Transport in a Polymer Electrolyte Membrane. *Nat. Mater.* **2011**, *10*, 507−511.

(3) Li, J.; Wilmsmeyer, K. G.; Hou, J.; Madsen, L. A. The Role of Water in Transport of Ionic Liquids in Polymeric Artificial Muscle Actuators. *Soft Matter* **2009**, *5*, 2596−2602.
(4) Pringle, J. M.; Howlett, P. C.; MacFarlane, D. R.; Forsyth, M. Organic Ionic Plastic Crystals: Recent Advances. *J. Mater. Chem.* **2010**, *20*, 2056−2062.
(5) Pringle, J. M. Recent Progress in the Development and Use of Organic Ionic Plastic Crystal Electrolytes. *Phys. Chem. Chem. Phys.* **2013**, *15*, 1339−1351.
(6) Lee, M.; Choi, U. H.; Wi, S.; Slebodnick, C.; Colby, R. H.; Gibson, H. W. 1,2-Bis[*N*-(*N*′-alkylimidazolium)]ethane Salts: a New Class of Organic Ionic Plastic Crystals. *J. Mater. Chem.* **2011**, *21*, 12280−12287.
(7) Lee, M.; Niu, Z.; Slebodnick, C.; Gibson, H. W. Structure and Properties of *N*,*N*-Alkylene Bis(*N*′-Alkylimidazolium) Salts. *J. Phys. Chem. B* **2010**, *114*, 7312−7319.
(8) Mehrer, H. *Diffusion in Solids: Fundamentals, Methods, Materials, Diffusion-Controlled Processes*; Springer Series in Solid-State Sciences; Springer: New York, 2007; Vol. *155*.
(9) Every, H. A.; Bishop, A. G.; MacFarlane, D. R.; Oradd, G.; Forsyth, M. Room Temperature Fast-ion Conduction in Imidazolium Halide Salts. *J. Mater. Chem.* **2001**, *11*, 3031−3036.
(10) Huang, J. H.; Hill, A.; Forsyth, M.; MacFarlane, D.; Hollenkamp, A. Conduction in Ionic Organic Plastic Crystals: the Role of Defects. *Solid State Ionics* **2006**, *177*, 2569−2573.
(11) Rana, U. A.; Vijayaraghavan, R.; MacFarlane, D. R.; Forsyth, M. Plastic Crystal Phases with High Proton Conductivity. *J. Mater. Chem.* **2012**, *22*, 2965−2974.
(12) Humphreys, F. J.; Hatherly, M. *Recrystallization and related annealing phenomena*; Elsevier: United Kingdom, 1995.
(13) Dosseh, G.; Fressigne, C.; Fuchs, A. H. Premelting in Orientationally Disordered Molecular Crystals. A Re-appraisal. *J. Phys. Chem. Solids* **1992**, *53*, 203−209.
(14) Chen, F.; de Leeuw, S. W.; Forsyth, M. Dynamic Heterogeneity and Ionic Conduction in an Organic Ionic Plastic Crystal and the Role of Vacancies. *J. Phys. Chem. Lett.* **2013**, *4*, 4085−4089.
(15) Lingwood, M. D.; Zhang, Z.; Kidd, B. E.; McCreary, K. B.; Hou, J.; Madsen, L. A. Unraveling the Local Energetics of Transport in a Polymer Ion Conductor. *Chem. Commun.* **2013**, *49*, 4283−4285.
(16) Commer, P.; Cherstvy, A. G.; Spohr, E.; Kornyshev, A. A. The Effects of Water Content on Proton Transport in Polymer Electrolyte Membranes. *Fuel Cells* **2003**, *2*, 127−136.
(17) Hou, J.; Zhang, Z.; Madsen, L. A. Cation/Anion Associations in Ionic Liquids Modulated by Hydration and Ionic Medium. *J. Phys. Chem. B* **2011**, *115*, 4576−4582.
(18) Urry, D. W. Henry Eyring (1901−1981): a 20th Century Physical Chemist and His Models. *Math. Modell.* **1982**, *3*, 503−522.
(19) Eyring, H. The Activated Complex in Chemical Reactions. *J. Chem. Phys.* **1935**, *3*, 107−115.
(20) Solomon, I. Multiple Echoes in Solids. *Phys. Rev.* **1958**, *110*, 61−65.
(21) Madsen, L. A.; Dingemans, T. J.; Nakata, M.; Samulski, E. T. Thermotropic Biaxial Nematic Liquid Crystals. *Phys. Rev. Lett.* **2004**, *92*, 145505−145509.
(22) Dingemans, T. J.; Madsen, L. A.; Zafiropoulos, N. A.; Lin, W. B.; Samulski, E. T. Uniaxial and Biaxial Nematic Liquid Crystals. *Philos. Trans. R. Soc., A* **2006**, *364*, 2681−2696.
(23) Stejskal, E.; Tanner, J. Spin Diffusion Measurements: Spin Echoes in the Presence of a Time−dependent Field Gradiet. *J. Chem. Phys.* **1965**, *42*, 288−292.
(24) Hou, J. B.; Madsen, L. A. New Insights for Accurate Chemically Specific Measurements of Slow Diffusing Molecules. *J. Chem. Phys.* **2013**, *138*, 054201-1−054201-8.
(25) Ashbrook, S. E.; Duer, M. J. Structural Information From Quadrupolar Nuclei in Solid State NMR. *Concepts Magn. Reson., Part A* **2006**, *28A*, 183−248.
(26) Li, J.; Wilmsmeyer, K. G.; Madsen, L. A. Anisotropic Diffusion and Morphology in Perfluorosulfonate Ionomers Investigated by NMR. *Macromolecules* **2009**, *42*, 255−262.
(27) Levitt, M. H. *Spin Dynamics*; John Wiley and Sons Ltd.: England, 2008; Vol. *2*.
(28) Collings, P. J. *Liquid Crystals: Nature's Delicate Phase of Matter*, 2nd ed.; Princeton University Press: New Jersey, 2002.
(29) Jin, L. Y.; Nairn, K. M.; Forsyth, C. M.; Seeber, A. J.; MacFarlane, D. R.; Howlett, P. C.; Forsyth, M.; Pringle, J. M. Structure and Transport Properties of a Plastic Crystal Ion Conductor: Diethyl(methyl)(isobutyl)phosphonium Hexafluorophosphate. *J. Am. Chem. Soc.* **2012**, *134*, 9688−2697.
(30) Adebahr, J.; Forsyth, M.; MacFarlane, D. R. Cation Dynamics in Dimethyl-pyrrolidinium-based Solid-state Ion Conductors. *Electrochim. Acta* **2005**, *50*, 3853−3858.
(31) P. G. de Gennes, J. P. *The Physics of Liquid Crystals*, 2nd ed.; Oxford Science Publications: New York, 1993.
(32) Callaghan, P. T. *Translational Dynamics Magnetic Resonance: Principles of Pulsed Gradient Spin Echo NMR*; Oxford University Press: New York, 2011.
(33) Callaghan, P. T.; Coy, A.; Macgowan, D.; Packer, K. J.; Zelaya, F. O. Diffraction-like Effects in NMR Diffusion Studies of Fluids in Porous Solids. *Nature* **1991**, *351*, 467−469.
(34) Hou, J.; Li, J.; Mountz, D.; Hull, M.; Madsen, L. A. Correlating Morphology, Proton Conductivity, and Water Transport in Polyelectrolyte-fluoropolymer Blend Membranes. *J. Membr. Sci.* **2013**, *448*, 292−299.
(35) Edward, J. T. Molecular Volumes and the Stokes-Einstein Equation. *J. Chem. Educ.* **1970**, *47*, 261−270.
(36) Einstein, A. On the Movement of Small Particles Suspended in Stationary Liquids Required by the Molecular-kinetic Theory of Heat. *Ann. Phys.* **1905**, *17*, 549−560.
(37) Chen, W. T.; Hsu, W. Y.; Lin, M. Y.; Tai, C. C.; Wang, S. P.; Sun, I. W. Isolated BMI^+ Cations are More than Isolated PF_6^- Anions in the Room Temperature 1-Butyl-3-methylimidazolium Hexafluorophosphate (BMI-PF_6) Ionic Liquid. *J. Chin. Chem. Soc.* **2010**, *57*, 1293−1298.
(38) Yu, G. R.; Zhao, D. C.; Wen, L.; Yang, S. D.; Chen, X. C. Viscosity of Ionic Liquids: Database, Observation, and Quantitative Structure-property Relationship Analysis. *AIChE J.* **2012**, *58*, 2885−2899.
(39) Adebahr, J.; Seeber, A. J.; MacFarlane, D. R.; Forsyth, M. LiI-Doped *N*,*N*-Dimethyl-pyrrolidinium Iodide, an Archetypal Rotator-Phase Ionic Conductor. *J. Phys. Chem. B* **2005**, *109*, 20087−20092.
(40) Forsyth, M.; Huang, J.; MacFarlane, D. R. Lithium Doped *N*-Methyl-*N*-ethylpyrrolidinium bis(trifluoromethanesulfonyl)amide Fast-ion Conducting Plastic Crystals. *J. Mater. Chem.* **2000**, *10*, 2259−2265.
(41) Howlett, P. C.; Sunarso, J.; Shekibi, Y.; Wasser, E.; Jin, L. Y.; MacFarlane, D. R.; Forsyth, M. On the Use of Organic Ionic Plastic Crystals in All Solid-state Lithium Methal Batteries. *Solid State Ionics* **2011**, *204*, 73−79.
(42) MacFarlane, D. R.; Forsyth, M. Plastic Crystal Electrolyte Materials: New Perspective on Solid State Ionics. *Adv. Mater.* **2001**, *13*, 957−966.
(43) MacFarlane, D. R.; Huang, J. H.; Forsyth, M. Lithium-Doped Plastic Crystal Electrolytes Exhibiting Fast Ion Conduction for Secondary Batteries. *Nature* **1999**, *402*, 792−794.